

# Spatial Downscaling of Streamflow Data with Attention Based Spatio-Temporal Graph Convolutional Networks

Muhammed Sit<sup>a\*</sup>, Bekir Z. Demiray<sup>a</sup>, Ibrahim Demir<sup>a,b,c</sup>

<sup>a</sup> IIHR Hydrosience and Engineering, University of Iowa, Iowa City, Iowa, USA

<sup>b</sup> Civil and Environmental Engineering, University of Iowa, Iowa City, Iowa, USA

<sup>c</sup> Electrical and Computer Engineering, University of Iowa, Iowa City, Iowa, USA

\* Corresponding Author, Email: [muhammed-sit@uiowa.edu](mailto:muhammed-sit@uiowa.edu)

## Abstract

Accurate streamflow data is vital for various climate modeling applications, including flood forecasting. However, many streams lack sufficient monitoring due to the high operational costs involved. To address this issue and promote enhanced disaster preparedness, management, and response, our study introduces a neural network-based method for estimating historical hourly streamflow in two spatial downscaling scenarios. The method targets two types of ungauged locations: (1) those without sensors in sparsely gauged river networks, and (2) those that previously had a streamflow sensor, but the gauge is no longer available. For both cases, we propose the ScaleGNN, a graph neural network based on Attention-Based Spatio-Temporal Graph Convolutional Networks (ASTGCN). We evaluate the performance of ScaleGNN against a Long Short-Term Memory (LSTM) baseline and spatial persistence in estimating discharge values over a 36-hour period. Our findings indicate that ScaleGNN surpasses spatial persistence in the first scenario, while both neural network approaches demonstrate their effectiveness compared to spatial persistence in the second scenario.

---

This manuscript is an EarthArXiv preprint that is not peer-reviewed or submitted to a journal. Subsequent versions of this manuscript may have slightly different content. Please feel free to contact the corresponding author for feedback.

---

## 1. Introduction

The development of flood risk assessment systems (Alabbad et al., 2022), operation of hydroelectric reservoirs, design of hydraulic structures, assessment of water quality (Demir et al., 2009), and long-term climate or land use change impacts are just a few of the many applications and studies that depend on accurate knowledge of streamflow. Similarly, prediction in ungauged basins (PUB) is one of the instances where the accuracy of out-of-sample forecasts matters the most (Xiang et al., 2021). From 2003 to 2012, PUB was the International Association of Hydrological Sciences' (IAHS) decadal problem (Hrachowitz et al., 2013; Sivapalan et al., 2003). Precise estimates of hydrological parameters like streamflow at ungauged sites enable quantitative and objective decision-making in water resource management (Demir and Beck, 2009) and disaster monitoring for smart cities of the future (Beck et al., 2010). Because ungauged basins lack data for model calibration and verification, hydrological regionalization is used to transfer information (e.g., model parameters) from gauged catchments (Blöschl and Sivapalan, 1995).

Streamflow forecasts from state-of-the-art regionalization, parameter transfer, catchment similarity, and surrogate basin techniques (Parajka et al., 2013; Razavi & Coulibaly, 2012; Samaniego et al., 2017) are less accurate than those from models calibrated separately in gauged catchments (Kratzert et al., 2019). At the moment, the best way to do PUB is to get detailed local knowledge of a basin (Blöschl, 2016), which is expensive for individual catchments and nearly impossible for simulations on a large scale. Vrugt et al. (2006) said that for lumped catchment models to give accurate estimates of streamflow, at least two to three years of gauge data are needed for calibration. Because the majority of streams in the world are either ungauged or inadequately gauged (Goswami et al., 2007; Sivapalan, 2003), and the number of gauged catchments, even in the United States, is diminishing, PUB remains a significant concern (Fekete et al., 2015).

One task that is quite similar to PUB is the estimation of current streamflow value in ungauged locations (i.e., downscaling or imputation of the data) as opposed to prediction of the stream parameters into the future. The goal in streamflow estimation study is to estimate hydrological model parameters for any grid cell or sub catchment without the requirement for model calibration or "tuning" to acquire the best match. Estimating streamflow for an ungauged basin or regionalizing an ungauged basin is often done by taking advantage of spatial proximity, physical similarity, regression-based methods, or hydrological signature methods. Besides these approaches, Guo et al. (2021) proposed a machine learning approach for this task, albeit its utilization is quite limited in the literature (Sit et al., 2022a).

Since floods are the primary disaster that affects human life on Earth, better disaster monitoring (Hu and Demir, 2021) and response for societal benefit depends on better flood forecasting. The National Weather Service (NWS) generates streamflow forecasts to oversee flooding for all locations that have United States Geological Survey (USGS) streamflow sensors. This is because their predictions of streamflow are based on measurements of streamflow from the past, which are not available for most communities. Therefore, in order to provide forecasts

for ungauged locations with no historical measurements, an alternative solution is to estimate historical streamflow for these locations and then use physical models. Furthermore, estimating streamflow in ungauged locations enables flood risk assessment (Yildirim and Demir, 2022), operation of hydroelectric reservoirs, and assessment of long-term climate, which in turn helps with better environmental and disaster monitoring.

## **1.1. Related Works**

### **1.1.1. Downscaling and Imputation of Hydrologic Data**

Even though there are studies that aim to estimate historical streamflow for ungauged locations with conceptual methods (Lorenz and Ziegewei, 2016), the literature over the imputation of hydrologic data using deep learning is quite limited. For this purpose, Hu et al. (2021) utilized variational mode decomposition and artificial neural networks for daily streamflow prediction in China. In a similar fashion, Nogueira Filho et al. (2022) explored long short-term memory (LSTM) networks for monthly streamflow estimation in Brazil. On the other hand, Hassan and Hassan (2020) improved ANN-based estimations using satellite snow-cover data. For daily streamflow estimations in a Mediterranean watershed, Oliveira et al. (2023) compared an ANN, a CNN, and an LSTM.

### **1.1.2. Prediction in Ungauged Basins**

On the other hand, PUB with machine learning and deep learning is widely explored in the literature. In one of such studies, for 7-day mean streamflow estimates, Worland et al. (2018) explored eight machine learning models, namely, elastic net, gradient boosting, k-nearest neighbors, random forest, two different support vector machines, and two different m5-cubist variations. They applied their methodology to 224 basins in the South United States and showed that many of the machine learning models they utilized are able to outperform four baseline models they've used, namely, ordinary kriging, a unit area discharge model, and two different variants of censored regression. For a similar exploration of machine learning models, Sikorska-Senoner and Quilty (2021) studied watersheds in Switzerland.

Beck et al. (2015) employed artificial neural networks (ANNs) for daily and monthly estimation of streamflow in thousands of watersheds globally. Similarly, for daily estimations in the United States, Atieh et al. (2017) utilized ANNs and gene expression programming (GEP). Razavi and Coulibaly (2017) followed a methodology that involves the spatial proximity and physical similarity of locations and river networks for the daily streamflow estimation of 90 watersheds in Ontario, Canada. They employed multi-layer perceptrons as well as support vector machines to estimate values targeting parameters of a hydrologic model. For a temporally harder target of hourly regionalization, Saadi et al. (2019) employed the random forest algorithm for more than 2,000 watersheds (of which 120 were pseudo-ungauged) in France and the United States. Employing deep learning in the prediction of ungauged basins has gained momentum in recent years. Kratzert et al. (2019) utilized LSTM networks for 531 watersheds from the CAMELS dataset. Similarly, Feng et al. (2020) trained LSTM models and showed that using

flow duration curves from nearby locations increases the accuracy of predictions. In an attempt to explore transfer learning for the same task, Oruche et al. (2021) trained LSTMs in which the network is first trained over data-rich regions and then fine-tuned over data-sparse regions. In a quite different methodology that aims to generate matrices instead of forecasting time-series, do Lago et al. (2023) utilized conditional generative adversarial networks (cGANs) to generate flood plains for certain flood scenarios.

### **1.1.3. Graph Neural Networks (GNNs) in Hydrology**

Utilization of graph neural networks in hydrological context has been appealing to domain scientists lately. While Sit et al. (2021) forecasted hourly streamflow for a basin in Iowa using upstream information, Xiang and Demir (2021) showed that a similar approach could be used to generalize forecasts for the whole state. In a similar approach, Jia et al. (2021) showed that recurrent graph models outperformed LSTM networks for both water flow and temperature in a transfer learning approach. In another comparative study, Ding et al. (2020) compared LSTMs with spatial and temporal attention to CNNs, Graph Convolutional Networks (GCNs), LSTMs, spatial attention LSTMs, and temporal attention LSTMs for basins in China. In another approach, Feng et al. (2021b) employed a spatially and temporally aware Graph Convolution Network (ST-GCN). They combined Graph Convolutional Networks (GCNs) and LSTMs for flood prediction for the Tunxi and Changhua River datasets. Finally, Sun et al. (2022) demonstrate how physics-based connectivity could be useful for PUB.

In this paper, the aim is to augment hourly streamflow datasets by estimating streamflow for locations in river networks without operational sensors for 36 hours. In order to do so, we utilized graph neural networks (GNNs), namely ScaleGNN, and compared it to a long short-term memory (LSTM) network. We also compared ScaleGNN and LSTM to spatial persistence, which was suggested by Krajewski et al. (2021) as a baseline for hydrological forecasting tasks. In order to understand how streamflow behaviors, change in river networks, we used node masking and marking methods to train the LSTM and the ScaleGNN. The latter is based on attention based spatial-temporal graph convolutional neural networks (Guo et al., 2019) for two kinds of ungauged locations: (1) ungauged locations with no sensors, which relies on generalizations over various river networks. Secondly, there are (2) ungauged locations that used to have a sensor but sensor is relocated or not active anymore for monitoring. To this end, we used WaterBench (Demir et al., 2022), which comprises discharge, precipitation, evapotranspiration, and various watershed characteristics, and built various river graphs throughout the State of Iowa.

The remainder of this paper is structured as follows: in the next section, we will define the research challenges we tackle, show how they could be conceptually solved, and describe the dataset that we use. In Section 3, we present the methods used in the study. Then, in Section 4, we present the experiment results and discuss the findings. Finally, Section 5 summarizes the findings of this study and shares prospects.

## 2. Methodology

### 2.1. Dataset and Problem Definition

In this section, we will define the problems we tackle in this study and give details as to how the dataset was facilitated to tackle defined problems. There are two use cases where the methodology in this study has applied: a) estimating streamflow at locations where there are no prior streamflow measurements and b) estimating streamflow at locations where there are historical streamflow measurements. A spatial persistence-based solution, which offers linear estimations, is utilized for both of use cases.

#### 2.1.1. Experimental Domain and Data

WaterBench (Demir et al., 2022) is a benchmark dataset designed for flood forecasting studies that follows FAIR data principles. The dataset is prepared with a focus on convenience for utilizing in data-driven and machine learning studies and provides benchmark performance for state-of-the-art deep learning architectures on the dataset for comparative analysis. By aggregating the datasets of streamflow, precipitation, watershed area, slope, soil types, and evapotranspiration from federal agencies and state organizations (i.e., NASA, NOAA, USGS, and the Iowa Flood Center), the WaterBench is prepared for hourly streamflow forecast studies. WaterBench provides data from 125 catchments in the State of Iowa. The precipitation time-series data ranges from October 2011 to September 2018. This dataset has a high temporal and spatial resolution with rich metadata and relational information, which can be used for a variety of deep learning and machine learning research (Sit et al., 2022b) and makes it a strong fit for the problem we tackle in this study.

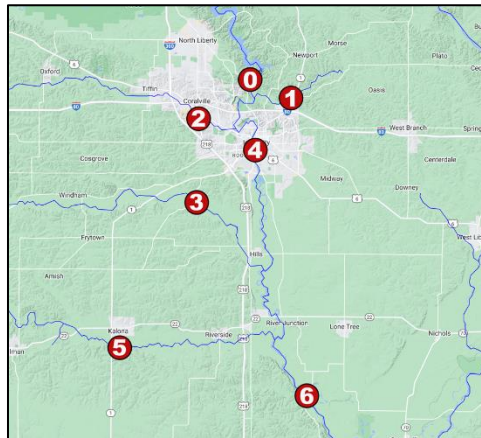


Figure 1. Sensor setup in and around Iowa City River at Iowa City.

Table 1. Experiment sensor IDs and their USGS IDs for Iowa City River at Iowa City.

ID	0	1	2	3	4	5	6
USGS ID	5453520	5454000	5454300	5455100	5454500	5455500	5455700

Table 2. Sensor pairs and water travel time between them for Iowa City River at Iowa City based on sensor IDs.

Sensor Pair	0 - 4	1 - 4	2 - 4	3 - 6	4 - 6	5 - 6
Travel Time (hr)	5	6	3	13	14	12

Even though WaterBench presents a large scale river network with 125 streamflow sensors throughout the state of Iowa, to provide a proof of concept, we chose three subsets of the Iowa river network, namely, the Iowa River Basin at Iowa City (Figure 1, Tables 1 and 2), the Des Moines River at Des Moines (Figure 2, Tables 3 and 4) and, the Cedar River Basin at Waterloo (Figure 3, Tables 5 and 6), each consisting of 7 streamflow sensors. These river networks were chosen for two reasons. The streamflow sensors on each of the river networks are located near highly populated areas with many tributaries, thus presenting a graph challenge. Since they are around highly populated areas, it is of utmost importance to estimate the streamflow values at ungauged locations, as flooding near populated areas affects daily life more.

Table 3. Experiment sensor IDs and their USGS IDs for Des Moines River at Des Moines.

ID	0	1	2	3	4	5	6
USGS ID	5481650	5484800	5481950	5482000	5484650	5484900	5485500

Table 4. Sensor pairs and water travel time between them for Des Moines River at Des Moines based on sensor IDs.

Sensor Pair	0 - 3	1 - 5	2 - 3	3 - 6	4 - 5	5 - 6
Travel Time (hr)	4	3	6	2	2	2

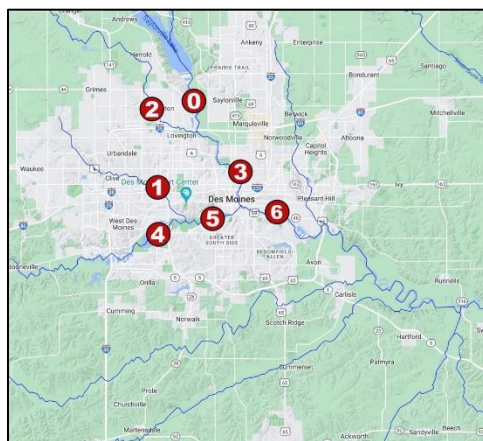


Figure 2. Sensor locations in and around Des Moines River at Des Moines.

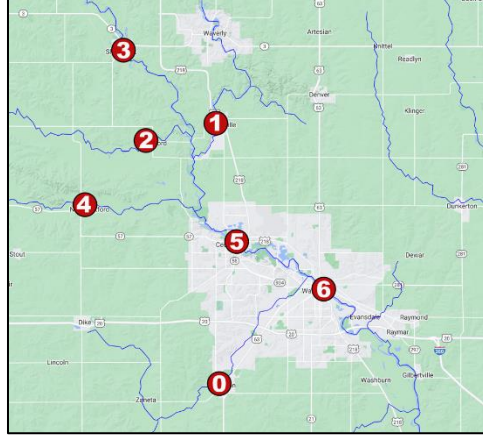


Figure 3. Sensor locations in and around Cedar River Basin at Waterloo.

Table 5. Experiment sensor IDs and their USGS IDs for Cedar River Basin at Waterloo.

<b>ID</b>	0	1	2	3	4	5	6
USGS ID	5463500	5458500	5458900	5462000	5463000	5463050	5464000

Table 6. Sensor pairs and water travel time between them for Cedar River Basin at Waterloo based on sensor IDs.

<b>Sensor Pair</b>	0 - 6	1 - 5	2 - 5	3 - 5	4 - 5	5 - 6
Travel Time (hr)	8	8	7	12	8	5

### 2.1.2. Problem Definition

This study aims to downscale streamflow measurements spatially. In order to address the questions using graph neural networks, river networks needed to be digitized in the graph format. In this study, we focus on three river networks. For simplicity purposes, each network is formed by seven USGS sensors. Edges are formed by their upstream-downstream relationships along with edge weights from the water’s travel time between them (Tables 2, 4, and 6).

In order to understand how streamflow behavior changes in river networks, this project aims to use node masking and node marking methods to train neural networks for two kinds of ungauged locations: (1) upstream nodes and (2) outlet/mainstream nodes. Thus, all the data was parsed for 36 hours of data for each of the sensors in each of the river networks, and dataset entries were formed by masking or marking each of the sensors. For each dataset entry, the time series sequence for one of the seven sensors is masked or marked by replacing them with zeros or calculated persistence values. In return, the output vector in each dataset entry has the actual values of the masked part of the input.

In summary, the goal of this study is to estimate streamflow values for locations where there are no operational streamflow sensors by utilizing measured streamflow values from neighboring sensors as well as rainfall and evapotranspiration (ET) data for the area. In this direction, we defined two use cases:

Use Case 1. Spatial Downscaling of Streamflow: This use case is broadly about estimating streamflow values for ungauged locations on a river network or a watershed using a neural network model that is trained to estimate streamflow sensor values for other river networks or watersheds. In other words, in this use case, a neural network trained using two watersheds and was tested on another watershed that it hadn't seen before. To this extent, in this use case, we trained a neural network model over two river networks, each with 7 sensors: the Iowa River in Iowa City, Iowa, United States, and the Des Moines River in Des Moines, Iowa, United States. For each dataset entry, there are values for discharge, evapotranspiration (ET), and rainfall for each of the sensors for 36 hours. So, the input array size is  $7 \times 3 \times 36$  (Figure 4). Instead of actual streamflow values for the "target" sensor (ungauged location on river network), we used calculated spatial persistence in the input. Spatial persistence was used with a small change in the approach as follows. Typically, spatial persistence calculations with multipoint estimations take the average of the contributions of multiple upstream locations. However, we empirically saw that, instead of averaging them, when we use the sum of the data that neural networks train over, performance increases. Thus, as a small preprocessing step, we used a modified version of the spatial persistence that we report in the training pipeline.

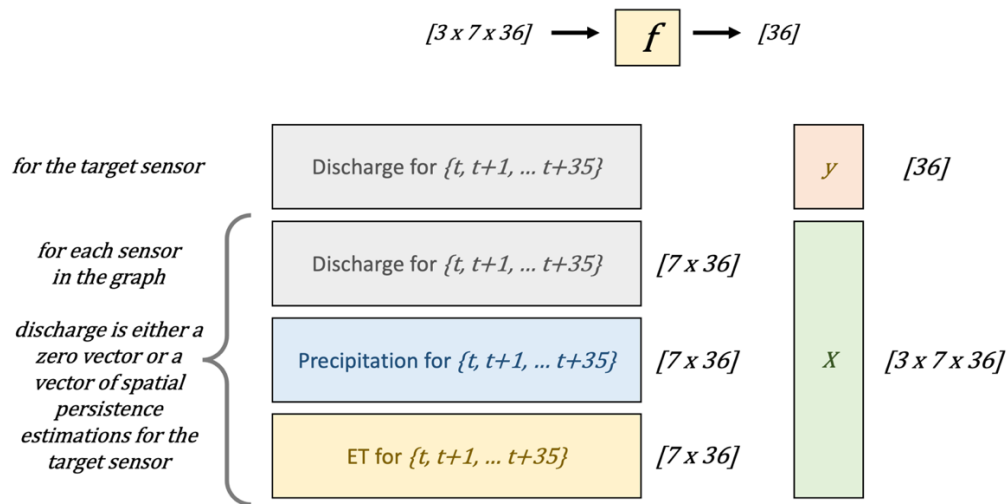


Figure 4. Input/Output details and shapes for the Graph Neural Network

Using such dataset entries, the neural network model learns to estimate the streamflow values for the sensor that was marked with calculated persistence instead of the real-world value, thus the output is a vector of size 36. Dataset entries are processed for each of the target sensors in the mentioned river networks for every timestamp that is available for all the sensors in the network. Testing is done for a river network in the Cedar River at Waterloo, Iowa, United States. For the most part, the goal in Use Case 1 was to explore the proposed neural network model's capabilities at estimating streamflow values for river networks it hadn't seen before to understand how a neural network generalizes.

Use Case 2. Temporal Imputation of Historical Streamflow: Use Case 2 uses the same marking strategy as Use Case 1, but the goal is slightly different because the neural network is trained and tested over the same river network. One other difference lies in the train-test split strategy. Throughout Use Case 2, we trained the LSTM baseline and the ScaleGNN using 5 years of streamflow data and tested over the data from the following 2 years. The overarching goal of this use case is to present a way to estimate streamflow values for locations that used to have operational streamflow sensors. Consequently, the model presented for this use case could be utilized to estimate streamflow at locations with streamflow gauges that are under maintenance or were simply discontinued as streamflow sensors are costly to operate.

We propose different workflows for Use Case 2, as it could be argued that it presents an easier challenge than Use Case 1 since it does not involve testing a model over a river network that hadn't been seen before and, consequently, it's a use case with more flexibility in terms of data needs. Both LSTM baseline and the ScaleGNN were trained over all the river networks mentioned in Use Case 1 for five years of data and tested over the remaining two years of data. Streamflow data for the target sensor is marked with calculated persistence. Same as before, but instead of marking the target sensor, the target sensor's discharge is "masked" with zeros.

## 2.2. Baseline Models

### 2.2.1. Spatial Persistence

Spatial persistence offers a linear estimation strategy for estimating stream measurements (or predictions) for a location on a river. There could be many ways to estimate streamflow with persistence, but the one we employed in this study ignores temporal dependencies and only uses basin sizes, historical streamflow measurements, and downstream-upstream relationships. In single point persistence estimations, to calculate spatial persistence for a location  $p$  on a river, one needs a location  $p'$  on the very same river with streamflow measurements such that the original location  $p$  has an upstream-downstream relationship. Aside from that, the only needed information would be the basin sizes for both locations ( $p$  and  $p'$ ). This process could be done using either downstream or upstream (but not both) relationships. For instance, in Figure 5, if the streamflow value of sensor 0 is known, the streamflow value of sensor 1 could be estimated by the Eq. 1.

$$d_1 = d_0 \frac{area_1}{area_0} \quad \text{Eq. 1}$$

The same formula can be used in reverse fashion, where the discharge of sensor 1 is known and that of sensor 0 is estimated as follows (Eq. 2):

$$d_0 = d_1 \frac{area_0}{area_1} \quad \text{Eq. 2}$$

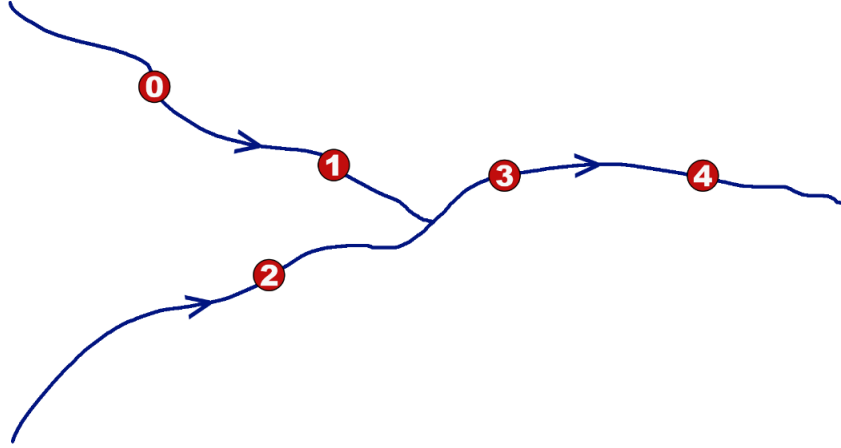


Figure 5. Demonstration of an experimental setup for spatial persistence estimations.

Even though single-point estimations can be done through either upstream or downstream connections, river networks are formed from branches, so multi-point estimations can be done from upstream connections. Again, from Figure 5, even though the spatial persistence of sensor 3 could be estimated through a downstream connection using sensor 4, it could also be estimated through an upstream connection with sensors 1 and 2 using the same formula (Eq. 3) with a small change:

$$d_3 = \left( d_1 \frac{area_3}{area_1} + d_2 \frac{area_3}{area_2} \right) / 2 \quad \text{Eq. 3}$$

In a reversed setting, one could only do a single-point estimation as one location does not feed water to two different downstream river branches. Spatial persistence sets a baseline for this study over the individual river networks. Each of the river networks was considered separate, and connections between them were ignored as the water travel times between the three sub-networks are significant and there are many streamflow sensors in between. For comparison purposes, we ran both spatial persistence (upstream and downstream) strategies whenever possible and saw that the strategy with the best outcome followed a scheme where downstream connections were preferential. If there is no downstream connection for a target sensor, then the upstream connections are used to estimate persistence. The results reported will be for the best-performing spatial persistence calculations given the circumstances.

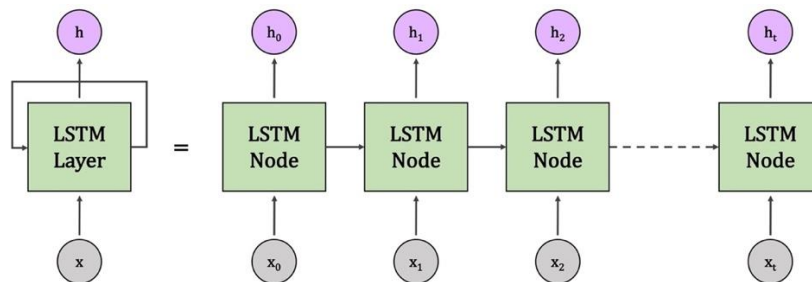


Figure 6. Structure and components of an LSTM layer

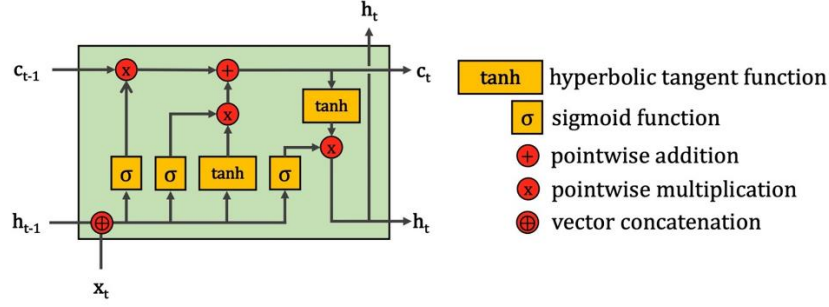


Figure 7. Structure and components of an LSTM node.

### 2.2.2. Long Short-Term Memory (LSTM) Networks

In recurrent neural networks (RNNs), memory vectors are trained at each step and then transferred to subsequent nodes or training stages. That is because the cumulative estimations and potential inferences that may be drawn from later parts of a time-series sequence may be impacted by the correlation of the overall time steps with the desired output. In order to capture the sequential nature of time series, this correlation of prior time steps with the output should be carried on to the following nodes. The data that is being learned and stored in a feature vector (a hidden state) in a "vanilla" RNN changes sporadically. The neural network's weight only receives a negligibly small amount of the gradient of the loss due to the vanishing gradient problem, which prevents learning. As a result, learning weights may lag behind or possibly come to an end. As a result, a straightforward and small RNN is unable to retain the learned properties over an extended period of time. This mostly affects how accurate time-series forecasts are.

$$i_t = \sigma(W^{(i)} x_t + U^{(i)} h_{t-1}) \quad \text{Eq. 4}$$

$$f_t = \sigma(W^{(f)} x_t + U^{(f)} h_{t-1}) \quad \text{Eq. 5}$$

$$o_t = \sigma(W^{(o)} x_t + U^{(o)} h_{t-1}) \quad \text{Eq. 6}$$

$$\tilde{c}_t = \tanh(W^{(c)} x_t + U^{(c)} h_{t-1}) \quad \text{Eq. 7}$$

$$c_t = f_t \circ c_{t-1} + i_t \circ \tilde{c}_{t-1} \quad \text{Eq. 8}$$

$$h_t = o_t \circ \tanh(c_t) \quad \text{Eq. 9}$$

In order to add more features to the deep neural network model, a long short-term memory neural network (Hochreiter and Schmidhuber, 1997) extends the lifespan of the short-term memory. In hydrological forecasting tasks that require longer memory, such as flood forecasting and rainfall forecasting, LSTMs and their variations are frequently used (Sit and Demir, 2019; Sit et al., 2022a). A concise description of an LSTM node and its mathematical foundation can be found in Equations 4 through 9, and Figures 6 and 7. Tensors  $x_t$  and  $h_{t-1}$  are given to an LSTM node, where  $x_t$  stands for the input and  $h_{t-1}$  for the hidden state of the layer's previous LSTM node. Equations 4 through 6 use  $\sigma$  to represent the sigmoid function, while  $\tanh$  in Equation 7 denotes the hyperbolic tangent function. The input gate (Eq. 4), forget gate (Eq. 5), output gate (Eq. 6), and cell update gate (Eq. 7) are formed, respectively, by the weight matrices

W and U, which modify the input and hidden state vectors. Because of these gates, LSTMs offer a mechanism for forgetting learned features from earlier nodes that are no longer relevant. The outputs of an LSTM node, which are  $c_t$  and  $h_t$ , are computed using these gates, where the  $\circ$  operator denotes the element-wise product. The hidden state of LSTM nodes, which is comparable to the hidden layer in RNNs, is where LSTM nodes store the information that will be needed right away while keeping the overall information in cell state (Eq. 8). The hidden state (Eq. 9) is then transmitted to the subsequent LSTM node and the subsequent layer in the neural network architecture, along with the cell state (Eq. 8).

Utilizing LSTM nodes, we built an LSTM-based neural network for comparison and benchmarking purposes. The LSTM-based neural network’s architecture details can be seen in Figure 8. Since the LSTM layers won’t train over the same data as the GNN, the data described in Figure 4 needed to be flattened into 21 channels, that is, 3 channels of data for each sensor in the river network, of time sequences with a length of 36. The fully connected layer that follows LSTM layers transforms the data into a sequence of 36 values, which are the estimations for the intended sensor.

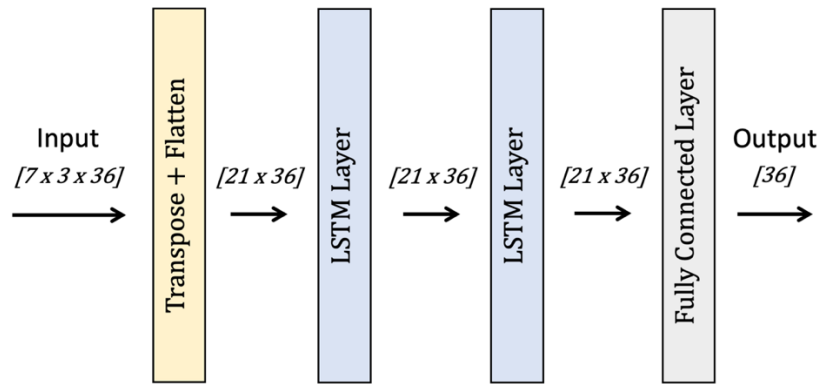


Figure 8. Architecture and details of the LSTM baseline

### 2.3. Attention Based Spatial-Temporal Graph Convolutional Networks (ASTGCN)

Sensors over river networks can be represented as directed graphs (Demir and Szczepanek, 2017). These sensors measure water that flows to other nodes in the network, along with contribution from other environmental factors such as rainfall. Since graph neural networks and graph convolutions take advantage of the spatial proximity and connections of nodes within graphs in modeling, GNNs are a good fit for streamflow studies. However, when temporal correlations are present, a standard GNN approach does not offer significant advantages. Forecasts or estimates considering spatial and temporal dependencies have been a challenge not only in streamflow but in other domains as well, such as traffic forecasting (Li et al., 2023; Tao et al., 2023) or traffic speed forecasts (Xu et al., 2021; Zhang et al., 2021). Recently, many deep-learning approaches have been proposed to overcome similar challenges, and models that are based on graph convolutional neural networks with additional components to capture a better

understanding of complex spatial and temporal relationships have gained lots of attention (Jiang and Luo, 2022; Wu et al., 2020).

One such example is the Spatio-Temporal Graph Convolutional Network (STGCN) (Yu et al., 2017), which was proposed for traffic prediction. In the model, two ST-blocks and one temporal convolutional layer are used. Each ST block contains two temporal gated convolution layers and one spatial graph convolution layer for temporal and spatial dependencies. Similarly, Guo et al. (2019) developed an Attention Based Spatial–Temporal Graph Convolution Network (ASTGCN) that improves the ST-Conv block by incorporating an attention layer to extract spatial-temporal features more effectively. Additionally, the model is divided into three sections, each considering historical data from the current day, one day prior, and one week prior. The output from each section was then combined through a fusion layer with corresponding weights. The experimental results suggested that including an attention layer could enhance the accuracy of the prediction model.

Encouraged by the success of GNNs in traffic forecasts and the similarity of traffic networks to river networks, in this study, a graph neural network architecture was chosen to be built, namely ScaleGNN, which is based on ASTGCN to estimate the historical streamflow values for 36 hours, only using the 36 hours of discharge, evapotranspiration, and rainfall values. Similar to the ASTGCN proposed for traffic forecasts, the ScaleGNN consists of multiple Spatial-Temporal Blocks (ST-Blocks), with each block containing attention and convolutional layers for both spatial and temporal correlations. To improve training efficiency, the model employs residual connections (He et al., 2016) between the input and output of each ST-Block. The design of the ScaleGNN is completed with a fully connected convolutional layer at the end of the last ST-Block. The general structure of the model is depicted in Figure 9.

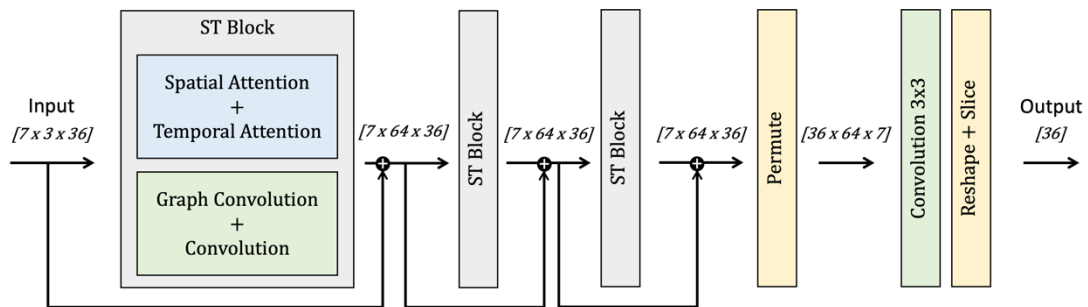


Figure 9. Architecture and component details of ScaleGNN

### 2.3.1. Spatial and Temporal Attention

The first part of the ST-Blocks are attention components. The attention mechanism provides a powerful way to learn which parts of the input data are most relevant for a particular task and has shown great promise in a wide range of applications (Niu et al., 2021; Brauwerters and Frasinca, 2021). Xu et al. (2015) introduced two attention mechanisms in the image description task and employed a visualization technique to demonstrate the impact of these attention mechanisms in a clear and intuitive manner. Vaswani et al. (2017) presented multi-head attention that enables the

model to attend to information from multiple representation subspaces simultaneously and at different positions. Velickovic et al. (2017) used the masked self-attention mechanism that works on graph-structured data and achieved state-of-the-art performance on four node classification benchmarks. In our case, two attention blocks are used, one for spatial and one for temporal dependencies in streamflow prediction.

Before going into the details, it is beneficial to provide some annotations. We denote the value of the  $c$ -th feature at time  $t$  on node  $i$  with  $x_t^{c,i}$ . Similarly, all feature values for node  $i$  at time  $t$  are denoted with  $x_t^i$ .  $X_t = (x_t^1, x_t^2, \dots, x_t^N)^T$  represents the values of all features on all nodes at time  $t$ .  $X = (X_1, X_2, \dots, X_T)^T$  denotes the values of all features on all nodes over  $T$  time slices.

**Spatial Attention:** In the spatial dimension, streamflow conditions at different sensors have a mutual influence on one another, and this influence is highly dynamic. To account for this, the model employs an attention mechanism (Feng et al. 2017) to flexibly capture the evolving correlations between nodes in the spatial dimension. The formula for spatial attention is provided below.

$$S = V_s \cdot \sigma\left((X_h^{r-1}W_1)W_2(W_3X_h^{r-1})^T + b_s\right) \quad \text{Eq. 10}$$

$$S'_{i,j} = \frac{\exp(S_{i,j})}{\sum_{j=1}^N \exp(S_{i,j})} \quad \text{Eq. 11}$$

In the Equation 10,  $X_h^{r-1} = (X_1, X_2, \dots, X_{T_{r-1}})$  represents the input of the  $r$ -th ST-Block. The length of the temporal axis is denoted by  $T_{r-1}$  in the  $r$ -th layer. The  $\sigma$  function is used as an activation function in the process, and  $V_s$ ,  $b_s$ ,  $W_1$ ,  $W_2$ , and  $W_3$  are all parameters that change during the process of learning the relationships. The matrix  $S$  that represents the correlation strength between nodes is computed dynamically based on the current input to the layer. Each element  $S_{i,j}$  in  $S$  denotes the correlation between node  $i$  and node  $j$ . The softmax function is applied so that the attention weights of a node are guaranteed to add up to one. During graph convolutions, the spatial attention matrix  $S'$  (Eq. 11) is combined with the adjacency matrix  $A$  to dynamically alter the weights of the nodes that impact each other.

**Temporal Attention:** Similar to spatial attention, the temporal relationship in the streamflow is extremely important, and it changes over time as a result of various factors. The attention mechanism is used to detect changes and determine the influence of each sensor on others over time. The mathematical relation for the temporal attention is provided in Equations 12 and 13.

$$E = V_e \cdot \sigma\left(((X_h^{r-1})^T U_1)U_2(U_3 X_h^{r-1}) + b_e\right) \quad \text{Eq. 12}$$

$$E'_{i,j} = \frac{\exp(E_{i,j})}{\sum_{j=1}^{T_{r-1}} \exp(E_{i,j})} \quad \text{Eq. 13}$$

The temporal correlation matrix is denoted by  $E$ , and  $E_{ij}$  represents the temporal correlation between times  $i$  and  $j$ . In the calculation of  $E$ , the weights of  $V_e$ ,  $U_1$ ,  $U_2$ ,  $U_3$ , and  $b_e$  are learnable and change over time. The softmax function is used to normalize the values as a last step in the calculation. The normalized temporal correlation matrix is merged with the input at the beginning of each ST-Block, and it dynamically provides temporal dependencies to model during the process.

### 2.3.2. Spatial and Temporal Convolutions

With the help of attention mechanisms, the network has the ability to highlight critical temporal and spatial dependencies and adjust the correlations. The input of the network, which is 36 hours of discharge, evapotranspiration, and rainfall values, is fed to attention layers to extract valuable information. More specifically, the input first enters the temporal layer, then moves to the spatial attention component. Once the input passes through attention layers, it goes to spatial and temporal convolution layers. In the network design, graph convolutional is used to capture spatial information from nearby sensors, and regular convolutional is preferred to acquire temporal dependencies from values with temporal proximity.

Spatial Convolutions: The spectral graph theory extends the concept of convolution from grid-based data to graphs. As mentioned, river networks are inherently graph structures, and each node in the network with its features can be viewed as a signal on the graph (Shuman et al., 2013). To make the most of the graph's topological properties, graph convolutions are applied at each time slice based on the spectral graph theory. By doing so, it is possible to utilize signal correlations on streamflow networks in the spatial dimension. Spectral graph theory is a way to analyze the topological attributes of a graph, such as connectivity in the graph structure, by transforming it into an algebraic form. This is done by representing the graph with its corresponding Laplacian matrix. The Laplacian matrix and its eigenvalues can be used to obtain the properties of the graph structure. Graph convolution is a convolution operation that is implemented using linear operators that diagonalize in the Fourier domain to replace the classical convolution operator (Henaff et al., 2015). However, it can be computationally expensive to perform eigenvalue decomposition on the Laplacian matrix for large-scale graphs. Therefore, Chebyshev polynomials are preferred to overcome this problem approximately but efficiently (Simonovsky and Komodakis 2017). Further details on the used graph convolutional layer can be found in Guo et al. (2019). The spatial convolution is completed with the ReLU activation function after the graph convolutional layer.

Temporal Convolution: After using graph convolution to capture information from neighboring nodes in the river network in the spatial dimension, a standard convolution layer is added in the temporal dimension to further update the node's signal by incorporating information from adjacent time slices. This allows the model to take into account how streamflow conditions are changing over time and capture temporal patterns in the data. After the standard convolution layer, ReLU is used as an activation layer.

In summary, similar to IGNNK (Wu et al., 2021), which is another GNN-based data imputation study, ScaleGNN uses three GNN blocks with residual connections. The GNN block in our case study is the ST-Block to capture both spatial and temporal correlations in data. Each ST-Block consists of attention and convolutional components that help to extract spatial and temporal features from the input data. To help with training efficiency, the model uses residual connections between the input and output of each ST-Block. This helps to ensure that the gradient can flow smoothly through the network during training. At the end of the last ST-Block, there is a fully connected convolutional layer that aggregates the extracted features from all the previous layers to produce the final output. Input and output shapes of each within the ScaleGNN could be seen in Figure 9, where the order of the Chebyshev polynomials is 3, and the number of Chebyshev filters and time filters is 64.

#### 2.4. Training and Testing Pipeline Details

Both the LSTM baseline and the ScaleGNN were trained using the same training pipeline, which employs the Adam optimizer with an early stopping mechanism that uses the patience of 10 epochs and no schedulers. The learning rate was adjusted between the LSTM baseline and ScaleGNN depending on their performances. Both networks were trained to minimize L1 loss using Nvidia TITAN V GPUs. Although the LSTM baseline was implemented in PyTorch, ScaleGNN also takes advantage of the Torch Geometric Temporal library on top of PyTorch.

#### 2.5. Evaluation Metrics

We calculated the estimation abilities of the described methods using a number of statistical variables. Here, we provide mean absolute error (MAE), Nash-Sutcliffe efficiency (NSE), and Kling-Gupta efficiency (KGE) as performance skill metrics.

Mean Absolute Error (MAE): The mean absolute error (MAE) or L1 loss represents the mean of the absolute difference between real and estimated values and can be seen in Eq. 14, where  $Q_o^t$  is the observed discharge and  $Q_m^t$  is the modeled discharge at time  $t$ . For each of the sensors over the test sets, estimations were generated by each of the methods, and their MAE scores were calculated against the ground truth of the very same sensor.

$$MAE = \frac{1}{n} \sum_{i=1}^n |Q_o^t - Q_m^t| \quad \text{Eq. 14}$$

Nash-Sutcliffe efficiency (NSE): The Nash-Sutcliffe efficiency (Eq. 15; NSE; Nash and Sutcliffe, 1970) assesses the performance between estimations of simulated discharge and gauged observations. NSE ranges from -inf to 1. The ideal value of NSE is equal to 1:

$$NSE = 1 - \frac{\sum_{t=1}^T (Q_o^t - Q_m^t)^2}{\sum_{t=1}^T (Q_o^t - \bar{Q}_o)^2} \quad \text{Eq. 15}$$

where  $Q_o^t$  is the observed discharge and  $Q_m^t$  is the modeled discharge at time  $t$ .  $\bar{Q}_o$  denotes the mean observed discharge.

**Kling-Gupta efficiency (KGE):** The Kling-Gupta efficiency (Gupta et al., 2009) is a modified form of the dimensionless NSE and assesses the performance between estimations of simulated discharge and gauged observations. The KGE metric consists of three parts (Eq. 16): Pearson's correlation  $r$ , standard deviation ratio, and mean ratio. The ideal value of KGE is equal to 1.

$$KGE = 1 - \sqrt{(r - 1)^2 + \left(\frac{\sigma_s}{\sigma_o} - 1\right)^2 + \left(\frac{\mu_s}{\mu_o} - 1\right)^2} \quad \text{Eq. 16}$$

where  $r$  is the linear correlation between discharge simulations and observations.  $\sigma_s$  denotes the standard deviation in simulations,  $\sigma_o$  the standard deviation in observations,  $\mu_s$  the mean of simulations, and  $\mu_o$  the mean of observations (equivalent to  $\bar{Q}_o$ ).

One should note that if the standard deviation ratio and the mean ratio are close to one, the KGE is dominated by the correlation coefficient  $r$ . Even though Knoben et al. (2019) showed that the interpretation of the KGE is more complex than the interpretation of Nash–Sutcliffe efficiency (NSE) values, mostly, KGE values above 0.75 suggest an outstanding simulation, whereas values between 0.5 and 0.75 indicate a reasonable simulation (Towner et al. 2019).

### 3. Results and Discussions

Using the described evaluation metrics, here we will present the results for each of the methods for two separate use cases. All results that will be shared here were acquired by running methods individually over the testing datasets for either of the use cases. For the neural networks, results for the best-performing neural network model over the mean absolute error over the testing dataset will be shared. As for the spatial persistence, the results of the best spatial persistence strategy, which uses downstream sensors for calculations wherever possible, will be presented. Another note is that, as we described in the experimental setting, for each target sensor, results were obtained using the actual discharge data for the 6 remaining sensors along with true precipitation and evapotranspiration data for all 7 sensors in the given river network.

Starting with Use Case 1, which is the spatial downscaling of streamflow in a river network that was not known by the method we are using, we share the average metrics for 36 hours of estimates. Table 7 shows all three metrics for all three methodologies. It should be noted that these scores were acquired by running each of the methods over each of the possible entries in the test dataset for each of the sensors, and then metrics were calculated for individual hours, as NSE and KGE formulations suggest. Finally, we took an average of 36 scores for each metric and reported them here. One could argue that hourly metrics should be shared, but since the use cases we tackle are for historical estimates rather than forecasts, one could also safely assume that the metrics would not change drastically over time. Our experiments have shown results to support this; thus, for the purposes of simplicity, we present averages rather than hourly metrics.

Table 7 clearly shows that ScaleGNN is significantly better than both the LSTM and Persistence baselines, being outperformed by the persistence by a slight margin in only two occurrences where it also provides results with a minor deficiency, that is, only in terms of KGE. This drastic difference between the LSTM and the ScaleGNN could be explained by the fact that while the ScaleGNN incorporates the graph nature of the river networks LSTM does not. Connections between sensor locations, along with distances between them are considered in the training for ScaleGNN and that new information would factor into estimations. Consequently, the graph information makes neural networks work well on a new river network that neither the LSTM nor the ScaleGNN have seen before, which is the driving factor of Use Case 1. Also, the ScaleGNN is significantly more complex than the LSTM in terms of the trainable parameters, but our experiments have shown that increasing the complexity with more layers for the LSTM does not necessarily improve the performance for this use case.

Table 7. Use Case 1 performance metrics of three methods for the test river network, the Cedar River Basin at Waterloo. The best scores for each row are highlighted in **bold**, and the second-best scores are underlined.

Sensor ID	Metric	StreamGNN	LSTM	Persistence
05463500	MAE	<b>163.5</b>	1353	<u>199.4</u>
	NSE	<b>0.516</b>	-6.850	<u>0.320</u>
	KGE	<b>0.470</b>	-3.184	<u>0.377</u>
05458500	MAE	<b>350.8</b>	1101	<u>420.0</u>
	NSE	<b>0.931</b>	0.307	<u>0.874</u>
	KGE	<b>0.930</b>	0.245	<u>0.859</u>
05458900	MAE	<b>237.4</b>	825.4	<u>258.5</u>
	NSE	<b>0.897</b>	0.171	<u>0.869</u>
	KGE	<b>0.906</b>	0.270	<u>0.877</u>
05462000	MAE	<b>343.0</b>	1068.9	<u>426.6</u>
	NSE	<b>0.914</b>	0.318	<u>0.832</u>
	KGE	<b>0.937</b>	0.270	<u>0.906</u>
05463000	MAE	<b>193.0</b>	1270	<u>223.5</u>
	NSE	<b>0.526</b>	-4.379	<u>0.415</u>
	KGE	<u>0.482</u>	-2.004	<b>0.484</b>
05463050	MAE	<b>300.0</b>	4683	<u>329.5</u>
	NSE	<b>0.991</b>	-0.300	<u>0.988</u>
	KGE	<u>0.960</u>	-0.123	<b>0.966</b>
05464000	MAE	<b>1266</b>	2925	<u>1612</u>
	NSE	<b>0.846</b>	0.308	<u>0.545</u>
	KGE	<b>0.772</b>	0.374	<u>0.728</u>

Table 8. Use Case 2 performances of three methods for the Iowa River Basin at Iowa City. The best scores for each row are highlighted in **bold**, and the second-best scores are underlined.

Sensor ID	Metric	StreamGNN		LSTM		Persistence
		w/ Persistence	Masked	w/ Persistence	Masked	
05453520	MAE	<b>143.6</b>	148.7	2235	181.7	<u>146.9</u>
	NSE	<b>0.989</b>	<b>0.989</b>	-1.063	0.979	<u>0.986</u>
	KGE	<b>0.966</b>	<u>0.955</u>	-0.271	0.953	<u>0.955</u>
05454000	MAE	73.80	<u>45.40</u>	272.0	86.80	<b>16.50</b>
	NSE	-2.118	<u>-0.721</u>	-110.9	-23.42	<b>0.032</b>
	KGE	-3.034	<u>-1.441</u>	-16.78	-4.861	<b>-0.081</b>
05454300	MAE	84.60	<u>56.00</u>	216.4	61.70	<b>52.50</b>
	NSE	-0.434	<b>0.087</b>	-27.76	-3.398	<u>0.045</u>
	KGE	-0.426	<b>0.264</b>	-4.696	-0.315	<u>0.153</u>
05455100	MAE	<b>90.00</b>	268.4	200.9	105.1	<u>103.4</u>
	NSE	<b>0.671</b>	-5.988	-2.263	-2.330	<u>0.303</u>
	KGE	<b>0.367</b>	-1.921	-0.585	-0.287	<u>0.248</u>
05454500	MAE	<u>260.6</u>	380.0	942.3	<b>166.0</b>	489.3
	NSE	<u>0.964</u>	0.929	0.494	<b>0.987</b>	0.837
	KGE	0.928	<u>0.955</u>	0.657	<b>0.965</b>	0.903
05455500	MAE	177.1	<u>174.3</u>	208.3	<b>125.1</b>	320.7
	NSE	0.741	<u>0.843</u>	0.624	<b>0.846</b>	0.376
	KGE	0.582	0.703	<u>0.770</u>	<b>0.894</b>	0.242
05455700	MAE	518.6	502.5	<u>453.0</u>	<b>322.1</b>	1343
	NSE	0.635	0.915	<u>0.952</u>	<b>0.972</b>	0.115
	KGE	0.655	0.858	<u>0.916</u>	<b>0.928</b>	0.462

For the most part, persistence already gives acceptable results in terms of NSE and KGE. While showing intermediate simulation for one sensor and outstanding simulation for four sensors, persistence is typically a viable option. Regardless, except for the USGS sensor 05463000, ScaleGNN improves the estimates significantly, resulting in outstanding simulations in 5 sensors and intermediate simulations in 2 sensors, one of which is a sensor where persistence is subpar.

For Use Case 2, both the LSTM baseline and the ScaleGNN were trained with 5 years of data from three river networks, and the best model for each over the MAE score using the test dataset, which consists of 2 years of data, was employed to acquire the scores presented. Tables 8-10 show the scores for each of the sensors in the Iowa River Basin at Iowa City, the Des Moines River at Des Moines, and the Cedar River Basin at Waterloo, respectively. We present two different sets of results for each of the neural networks (with Persistence and Masked) to show if neural networks build on top of already-given persistence or not.

Table 9. Use Case 2 performances of three methods for the Des Moines River at Des Moines. The best scores for each row are highlighted in **bold**, and the second-best scores are underlined.

Sensor ID	Metric	StreamGNN		LSTM		Persistence
		w/ Persistence	Masked	w/ Persistence	Masked	
05481650	MAE	<u>402.1</u>	488.3	4598	488.2	<b>290.3</b>
	NSE	<u>0.987</u>	0.974	-0.408	0.981	<b>0.993</b>
	KGE	<u>0.985</u>	0.942	0.088	0.980	<b>0.991</b>
05484800	MAE	108.0	<u>96.40</u>	2334	122.2	<b>61.20</b>
	NSE	<b>0.255</b>	0.093	-208.4	-0.115	<u>0.131</u>
	KGE	-0.092	-0.062	-27.90	<b>0.285</b>	<u>0.036</u>
05481950	MAE	197.6	<b>167.6</b>	1857	<u>178.8</u>	260.0
	NSE	<u>0.554</u>	<b>0.592</b>	-35.25	0.417	0.310
	KGE	<u>0.587</u>	0.531	-6.114	<b>0.650</b>	0.388
05482000	MAE	<u>772.2</u>	1330	1103	<b>383.1</b>	1284
	NSE	<u>0.945</u>	0.848	0.867	<b>0.987</b>	0.893
	KGE	<u>0.892</u>	0.782	0.868	<b>0.945</b>	0.836
05484650	MAE	<u>276.0</u>	311.6	926.2	288.4	<b>212.5</b>
	NSE	<b>0.982</b>	0.978	0.759	0.975	<u>0.980</u>
	KGE	<b>0.971</b>	0.963	0.798	<u>0.966</u>	0.903
05484900	MAE	664.8	858.0	<u>514.2</u>	<b>279.3</b>	1107
	NSE	0.911	0.804	<u>0.932</u>	<b>0.982</b>	0.756
	KGE	<b>0.941</b>	0.698	0.915	<u>0.940</u>	0.764
05485500	MAE	583.4	1044	<u>456.3</u>	<b>420.7</b>	707.3
	NSE	<u>0.990</u>	0.950	<b>0.993</b>	<b>0.993</b>	0.980
	KGE	0.973	0.875	<b>0.987</b>	<u>0.986</u>	0.952

Overall, both neural network approaches perform similarly; if one of them has an NSE or KGE of more than 0.5, the other performs similarly for the most part. The numbers of sensors that each neural network approach performs better than the others seem to be distributed almost evenly.

In the Iowa River Basin at Iowa City network, except for one sensor, persistence is outperformed by neural network models. For two sensors with small basins in the same river network, 05454000 and 05454300, none of the methods seem to be simulating well enough. Regardless, it would be fair to state that LSTM tends to be better in larger basins, whereas StreamGNN could be slightly better in smaller basins while providing intermediate results in larger basins.

Table 10. Use Case 2 performances of three methods for the Cedar River Basin at Waterloo. The best scores for each row are highlighted in **bold**, and the second-best scores are underlined.

Sensor ID	Metric	StreamGNN		LSTM		Persistence
		w/ Persistence	Masked	w/ Persistence	Masked	
05463500	MAE	<u>170.1</u>	184.0	1075	<b>147.5</b>	200.4
	NSE	0.113	-0.105	-17.81	<b>0.489</b>	<u>0.304</u>
	KGE	<u>0.513</u>	0.46.0	-3.677	<b>0.627</b>	0.431
05458500	MAE	<b>430.0</b>	<u>438.9</u>	922.9	523.0	482.4
	NSE	<b>0.916</b>	<u>0.912</u>	0.522	0.869	0.872
	KGE	<u>0.882</u>	0.845	0.675	<b>0.897</b>	0.841
05458900	MAE	<b>261.7</b>	298.3	894.1	<u>265.7</u>	273.8
	NSE	<b>0.911</b>	0.872	-0.775	0.848	<u>0.884</u>
	KGE	<b>0.927</b>	0.838	0.107	0.819	<u>0.859</u>
05462000	MAE	543.8	<u>514.0</u>	1042	547.4	<b>440.2</b>
	NSE	0.810	<b>0.847</b>	0.307	0.828	<u>0.844</u>
	KGE	0.722	<u>0.770</u>	0.548	0.768	<b>0.885</b>
05463000	MAE	<u>196.9</u>	262.7	1163	<b>178.1</b>	210.0
	NSE	<b>0.524</b>	-0.663	-14.99	0.352	<u>0.506</u>
	KGE	<u>0.624</u>	0.046	-3.020	<b>0.648</b>	0.561
05463050	MAE	<u>295.2</u>	418.7	3994	<b>251.4</b>	342.8
	NSE	<b>0.994</b>	0.988	0.233	<b>0.994</b>	<u>0.991</u>
	KGE	<u>0.970</u>	0.964	0.313	<b>0.990</b>	0.953
05464000	MAE	744.7	772.2	<u>370.4</u>	<b>296.7</b>	1616
	NSE	0.948	0.938	<u>0.986</u>	<b>0.993</b>	0.806
	KGE	0.936	0.858	<b>0.973</b>	<u>0.969</u>	0.831

In the Des Moines River at Des Moines, even though there are still simulations with unacceptable performances for a sensor, it looks better for neural networks. The LSTM-based neural network, predominantly, continues to outperform ScaleGNN in larger basins. While persistence gets scores that are good enough for a linear model, it lacks a good mean absolute error for larger basins. In the Cedar River Basin at Waterloo, similar trends continue. Except for the first sensor, which is a small basin, both neural network models provide at least acceptable performances for the data imputation task.

For the most part, the performance differences between the ScaleGNN with persistence input and the one with masked input suggest that ScaleGNN was able to improve performance using persistence data as a starting point. On the other hand, the LSTM-based neural network mostly didn't perform well at all with the persistence input while performing on par with ScaleGNN, which uses persistence input. Overall, it could be argued that for Use Case 2, LSTMs are generally a better fit than the ScaleGNN as they have lower memory needs than the ScaleGNN

we propose. However, it should be noted that LSTMs mostly outperform the ScaleGNN in larger basins. If the data imputation task is for smaller basins, in other words, if the estimates are for a small basin that does not have a working sensor anymore, given the training is done for the entirety of the river network, ScaleGNN could be the better choice.

#### **4. Conclusions**

In this study, we defined two problems. First, we described the problem of spatial downscaling of streamflow measurements, or, in other words, estimating streamflow for new locations in a known river network without means of sensing. Secondly, we defined a problem where a sensor in a river network goes out of commission and the new streamflow levels need to be estimated. For both of these problems, we first showed that they could be tackled linearly with spatial persistence, and then we showed that they could be further resolved using LSTMs and a graph neural network based on Attention Based Spatial-Temporal Graph Convolutional Networks (ASTGCN), namely ScaleGNN. Our results clearly showed that ScaleGNN improves over the spatial persistence for the first use case, while both LSTM and ScaleGNN show promising results for the second use case.

In the future, we plan to apply this study to the whole WaterBench dataset to see how trained models can be used in different situations over a large set of sensor network. Also, we plan on developing a data preprocessing pipeline to include graph information in the input that was fed to the LSTM-based neural network to see if LSTMs could perform as well as the ScaleGNN over the river networks for which they have not been trained.

#### **References**

- Alabbad, Y., Yildirim, E. and Demir, I., 2022. Flood mitigation data analytics and decision support framework: Iowa Middle Cedar Watershed case study. *Science of The Total Environment*, 814, p.152768.
- Atieh, M., Taylor, G., Sattar, A.M. and Gharabaghi, B., 2017. Prediction of flow duration curves for ungauged basins. *Journal of hydrology*, 545, pp.383-394.
- Beck, M.B., Jiang, F., Shi, F., Walker, R.V., Osidele, O.O., Lin, Z., Demir, I. and Hall, J.W., 2010. Re-engineering cities as forces for good in the environment. In *Proceedings of the Institution of Civil Engineers-Engineering Sustainability (Vol. 163, No. 1, pp. 31-46)*.
- Beck, H.E., De Roo, A. and van Dijk, A.I., 2015. Global maps of streamflow characteristics based on observations from several thousand catchments. *Journal of Hydrometeorology*, 16(4), pp.1478-1501.
- Blöschl, G. and Sivapalan, M., 1995. Scale issues in hydrological modelling: a review. *Hydrological processes*, 9(3-4), pp.251-290.
- Blöschl, G., 2016. Predictions in ungauged basins—where do we stand?. *Proceedings of the International Association of Hydrological Sciences*, 373, pp.57-60.
- Brauwiers, G. and Frasincar, F., 2021. A general survey on attention mechanisms in deep learning. *IEEE Transactions on Knowledge and Data Engineering*.

- Demir, I. and Beck, M.B., 2009, April. GWIS: a prototype information system for Georgia watersheds. In Georgia Water Resources Conference: Regional Water Management Opportunities, UGA, Athens, GA, US.
- Demir, I., Jiang, F., Walker, R. V., Parker, A. K., & Beck, M. B. 2009. Information systems and social legitimacy scientific visualization of water quality. In 2009 IEEE International Conference on Systems, Man and Cybernetics (pp. 1067-1072). IEEE.
- Demir, I. and Szczepanek, R., 2017. Optimization of river network representation data models for web-based systems. *Earth and Space Science*, 4(6), pp.336-347.
- Demir, I., Xiang, Z., Demiray, B. and Sit, M., 2022. WaterBench-Iowa: a large-scale benchmark dataset for data-driven streamflow forecasting. *Earth system science data*, 14(12), pp.5605-5616.
- Ding, Y., Zhu, Y., Feng, J., Zhang, P. and Cheng, Z., 2020. Interpretable spatio-temporal attention LSTM model for flood forecasting. *Neurocomputing*, 403, pp.348-359.
- do Lago, C. A. F. et al. (2023) 'Generalizing rapid flood predictions to unseen urban catchments with conditional generative adversarial networks', *Journal of Hydrology*, 618, p. 129276. doi: 10.1016/j.jhydrol.2023.129276.
- Fekete, B.M., Robarts, R.D., Kumagai, M., Nachtnebel, H.P., Odada, E. and Zhulidov, A.V., 2015. Time for in situ renaissance. *Science*, 349(6249), pp.685-686.
- Feng, D., Lawson, K. and Shen, C., 2020. Prediction in ungauged regions with sparse flow duration curves and input-selection ensemble modeling. arXiv preprint arXiv:2011.13380.
- Feng, J., Wang, Z., Wu, Y. and Xi, Y., 2021b, July. Spatial and Temporal Aware Graph Convolutional Network for Flood Forecasting. In 2021 International Joint Conference on Neural Networks (IJCNN) (pp. 1-8). IEEE.
- Feng, X., Guo, J., Qin, B., Liu, T. and Liu, Y., 2017, August. Effective Deep Memory Networks for Distant Supervised Relation Extraction. In IJCAI (Vol. 17, pp. 1-7).
- Goswami, M., O'connor, K.M. and Bhattarai, K.P., 2007. Development of regionalisation procedures using a multi-model approach for flow simulation in an ungauged catchment. *Journal of Hydrology*, 333(2-4), pp.517-531.
- Guo, S., Lin, Y., Feng, N., Song, C. and Wan, H., 2019, July. Attention based spatial-temporal graph convolutional networks for traffic flow forecasting. In Proceedings of the AAAI conference on artificial intelligence (Vol. 33, No. 01, pp. 922-929).
- Guo, Y., Zhang, Y., Zhang, L. and Wang, Z., 2021. Regionalization of hydrological modeling for predicting streamflow in ungauged catchments: A comprehensive review. *Wiley Interdisciplinary Reviews: Water*, 8(1), p.e1487.
- Hassan, M. and Hassan, I., 2020. Improving ANN-based streamflow estimation models for the Upper Indus Basin using satellite-derived snow cover area. *Acta Geophysica*, 68(6), pp.1791-1801.
- He, K., Zhang, X., Ren, S. and Sun, J., 2016. Deep residual learning for image recognition. In Proceedings of the IEEE conference on computer vision and pattern recognition (pp. 770-778).

- Henaff, M., Bruna, J. and LeCun, Y., 2015. Deep convolutional networks on graph-structured data. arXiv preprint arXiv:1506.05163.
- Hrachowitz, M., Savenije, H.H.G., Blöschl, G., McDonnell, J.J., Sivapalan, M., Pomeroy, J.W., Arheimer, B., Blume, T., Clark, M.P., Ehret, U. and Fenicia, F., 2013. A decade of Predictions in Ungauged Basins (PUB)—a review. *Hydrological sciences journal*, 58(6), pp.1198-1255.
- Hu, A. and Demir, I., 2021. Real-time flood mapping on client-side web systems using hand model. *Hydrology*, 8(2), p.65.
- Hu, H., Zhang, J. and Li, T., 2021. A Novel Hybrid Decompose-Ensemble Strategy with a VMD-BPNN Approach for Daily Streamflow Estimating. *Water Resources Management*, 35(15), pp.5119-5138.
- Jia, X., Zwart, J., Sadler, J., Appling, A., Oliver, S., Markstrom, S., Willard, J., Xu, S., Steinbach, M., Read, J. and Kumar, V., 2020. Physics-guided recurrent graph networks for predicting flow and temperature in river networks. arXiv preprint arXiv:2009.12575.
- Jiang, W. and Luo, J., 2022. Graph neural network for traffic forecasting: A survey. *Expert Systems with Applications*, p.117921.
- Knoben, W.J., Freer, J.E. and Woods, R.A., 2019. Inherent benchmark or not? Comparing Nash–Sutcliffe and Kling–Gupta efficiency scores. *Hydrology and Earth System Sciences*, 23(10), pp.4323-4331.
- Krajewski, W.F., Ghimire, G.R., Demir, I. and Mantilla, R., 2021. Real-time streamflow forecasting: AI vs. Hydrologic insights. *Journal of Hydrology X*, 13, p.100110.
- Kratzert, F., Klotz, D., Herrnegger, M., Sampson, A.K., Hochreiter, S. and Nearing, G.S., 2019. Toward improved predictions in ungauged basins: Exploiting the power of machine learning. *Water Resources Research*, 55(12), pp.11344-11354.
- Liu, M., Liu, G. and Sun, L., 2023. Spatial-Temporal Dependence and Similarity Aware Traffic Flow Forecasting. *Information Sciences*.
- Lorenz, D.L. and Ziegeweid, J.R., 2016. Methods to estimate historical daily streamflow for ungauged stream locations in Minnesota (No. 2015-5181). US Geological Survey.
- Nash, J.E. and Sutcliffe, J.V., 1970. River flow forecasting through conceptual models part I—A discussion of principles. *Journal of hydrology*, 10(3), pp.282-290.
- Niu, Z., Zhong, G. and Yu, H., 2021. A review on the attention mechanism of deep learning. *Neurocomputing*, 452, pp.48-62.
- Nogueira Filho, F.J.M., Souza Filho, F.D.A., Porto, V.C., Vieira Rocha, R., Sousa Estácio, Á.B. and Martins, E.S.P.R., 2022. Deep Learning for Streamflow Regionalization for Ungauged Basins: Application of Long-Short-Term-Memory Cells in Semiarid Regions. *Water*, 14(9), p.1318.
- Oliveira, A.R., Ramos, T.B. and Neves, R., 2023. Streamflow Estimation in a Mediterranean Watershed Using Neural Network Models: A Detailed Description of the Implementation and Optimization. *Water*, 15(5), p.947.

- Oruche, R., Egede, L., Baker, T. and O'Donncha, F., 2021. Transfer learning to improve streamflow forecasts in data sparse regions. arXiv preprint arXiv:2112.03088.
- Parajka, J., Viglione, A., Rogger, M., Salinas, J.L., Sivapalan, M. and Blöschl, G., 2013. Comparative assessment of predictions in ungauged basins—Part 1: Runoff-hydrograph studies. *Hydrology and Earth System Sciences*, 17(5), pp.1783-1795.
- Razavi, T. and Coulibaly, P., 2017. An evaluation of regionalization and watershed classification schemes for continuous daily streamflow prediction in ungauged watersheds. *Canadian Water Resources Journal/Revue canadienne des ressources hydriques*, 42(1), pp.2-20.
- Saadi, M., Oudin, L. and Ribstein, P., 2019. Random forest ability in regionalizing hourly hydrological model parameters. *Water*, 11(8), p.1540.
- Shuman, D.I., Narang, S.K., Frossard, P., Ortega, A. and Vandergheynst, P., 2013. The emerging field of signal processing on graphs: Extending high-dimensional data analysis to networks and other irregular domains. *IEEE signal processing magazine*, 30(3), pp.83-98.
- Sikorska-Senoner, A.E. and Quilty, J.M., 2021. A novel ensemble-based conceptual-data-driven approach for improved streamflow simulations. *Environmental Modelling & Software*, 143, p.105094.
- Simonovsky, M. and Komodakis, N., 2017. Dynamic edge-conditioned filters in convolutional neural networks on graphs. In *Proceedings of the IEEE conference on computer vision and pattern recognition* (pp. 3693-3702).
- Sit, M. and Demir, I., 2019. Decentralized flood forecasting using deep neural networks. arXiv preprint arXiv:1902.02308.
- Sit, M., Demiray, B., & Demir, I. 2021. Short-term hourly streamflow prediction with graph convolutional gru networks. arXiv preprint arXiv:2107.07039.
- Sit, M., Demiray, B.Z. and Demir, I., 2022a. A Systematic Review of Deep Learning Applications in Streamflow Data Augmentation and Forecasting. *EarthArxiv*, 3617. <https://doi.org/10.31223/X5HM08>
- Sit, M., Demiray, B.Z. and Demir, I., 2022b. A Systematic Review of Deep Learning Applications in Interpolation and Extrapolation of Precipitation Data. *EarthArxiv*, 4715. <https://doi.org/10.31223/X57H2H>
- Sivapalan, M., 2003. Prediction in ungauged basins: a grand challenge for theoretical hydrology. *Hydrological processes*, 17(15), pp.3163-3170.
- Sun, A.Y., Jiang, P., Yang, Z.L., Xie, Y. and Chen, X., 2022. A graph neural network approach to basin-scale river network learning: The role of physics-based connectivity and data fusion. *Hydrology and Earth System Sciences Discussions*, pp.1-35.
- Tao, S., Zhang, H., Yang, F., Wu, Y. and Li, C., 2023. Multiple Information Spatial-Temporal Attention Based Graph Convolution Network for traffic prediction. *Applied Soft Computing*, p.110052.
- Towner, J., Cloke, H.L., Zsoter, E., Flamig, Z., Hoch, J.M., Bazo, J., Coughlan de Perez, E. and Stephens, E.M., 2019. Assessing the performance of global hydrological models for

- capturing peak river flows in the Amazon basin. *Hydrology and Earth System Sciences*, 23(7), pp.3057-3080.
- Vaswani, A., Shazeer, N., Parmar, N., Uszkoreit, J., Jones, L., Gomez, A.N., Kaiser, Ł. and Polosukhin, I., 2017. Attention is all you need. *Advances in neural information processing systems*, 30.
- Veličković, P., Cucurull, G., Casanova, A., Romero, A., Lio, P. and Bengio, Y., 2017. Graph attention networks. *arXiv preprint arXiv:1710.10903*.
- Vrugt, J.A., Gupta, H.V., Dekker, S.C., Sorooshian, S., Wagener, T. and Bouten, W., 2006. Application of stochastic parameter optimization to the Sacramento Soil Moisture Accounting model. *Journal of Hydrology*, 325(1-4), pp.288-307.
- Worland, S.C., Farmer, W.H. and Kiang, J.E., 2018. Improving predictions of hydrological low-flow indices in ungaged basins using machine learning. *Environmental modelling & software*, 101, pp.169-182.
- Wu, Y., Zhuang, D., Labbe, A. and Sun, L., 2021, May. Inductive graph neural networks for spatiotemporal kriging. In *Proceedings of the AAAI Conference on Artificial Intelligence*(Vol. 35, No. 5, pp. 4478-4485).
- Wu, Z., Pan, S., Chen, F., Long, G., Zhang, C. and Philip, S.Y., 2020. A comprehensive survey on graph neural networks. *IEEE transactions on neural networks and learning systems*, 32(1), pp.4-24.
- Xiang, Z. and Demir, I., 2021. High-resolution rainfall-runoff modeling using graph neural network. *arXiv preprint arXiv:2110.10833*.
- Xiang, Z., Demir, I., Mantilla, R. and Krajewski, W.F., 2021. A regional semi-distributed streamflow model using deep learning. *EarthArxiv*, 2152. <https://doi.org/10.31223/X5GW3V>
- Xu, K., Ba, J., Kiros, R., Cho, K., Courville, A., Salakhudinov, R., Zemel, R. and Bengio, Y., 2015, June. Show, attend and tell: Neural image caption generation with visual attention. In *International conference on machine learning* (pp. 2048-2057). PMLR.
- Xu, Y., Liu, W., Jiang, Z., Xu, Z., Mao, T., Chen, L. and Zhou, M., 2021. MAF-GNN: Multi-adaptive spatiotemporal-flow graph neural network for traffic speed forecasting. *arXiv preprint arXiv:2108.03594*.
- Yildirim, E. and Demir, I., 2022. Agricultural flood vulnerability assessment and risk quantification in Iowa. *Science of The Total Environment*, 826, p.154165.
- Yu, B., Yin, H. and Zhu, Z., 2017. Spatio-temporal graph convolutional networks: A deep learning framework for traffic forecasting. *arXiv preprint arXiv:1709.04875*.
- Zhang, Z., Li, Y., Song, H. and Dong, H., 2021. Multiple dynamic graph based traffic speed prediction method. *Neurocomputing*, 461, pp.109-117.